Features of glacial valley profiles simply explained

Robert S. Anderson,[1] Peter Molnar,[2] and Mark A. Kessler[3]

[1] Glacial occupation of alpine valleys results in a distinct signature in the long-valley profile, including steepening of the profile in the headwaters, flattening at lower elevations, and a step in the profile at the convergence of headwater tributaries. We present analytic results for glacial erosion patterns by making the following assumptions: (1) the initial profile is linear, (2) the width of the valley is uniform, (3) the annual mass balance varies linearly with elevation, (4) the glacier at any time is quasi-steady, (5) the erosion rate is proportional to ice discharge per unit valley width, and (6) glacial erosion rates far exceed fluvial erosion rates. A steady glacier under these conditions would erode a parabolic divot in the longitudinal valley profile, with its maximum depth coinciding with the down-valley position of the equilibrium line altitude (ELA). The calculated flattening of the valley floor down valley of the ELA and the steepening of it up valley captures the essence of the glacial signature. When a reasonable probability distribution of ELAs is allowed, the predicted erosion peaks at 30–40% of the down-valley distance to the glacial limit, and the pattern merges smoothly with the steeper fluvial profile downstream of the glacial limit. Profiles of mass balance that are capped at a maximum value produce shorter glaciers and a slight asymmetry in the expected erosion pattern. Only when we mimic the tributaries of glacial headwaters by specifying a valley width distribution do we obtain the upper step observed in many valley profiles.

1. Introduction

[2] Alpine glaciers are efficient erosional engines that occupy both former stream channels and valley walls. Therefore they overprint fluvial valleys with a signature of glacial advance across the entire alpine landscape. The Plio-Pleistocene climate [e.g., *Raymo*, 1994] has driven dozens of cycles of glacial advance and retreat in alpine valleys that have shaped a landscape very different from those in which rivers are the main erosive agent, and from the landscape that existed before glaciation became common in the Ice Age. Our goal is to understand the erosional legacy of glacial advances and retreats in alpine valleys in terms of simple characteristics of glaciers and their differences from rivers as erosional agents.

[3] Herein, we formalize and build upon the conceptual models of previous researchers [e.g., *Penck*, 1905; *Sugden and John*, 1976] that provide an intuitive understanding of how climate, topography and glacial erosion result in the gross characteristics of longitudinal valley profiles. The development of an analytical/numerical model is crucial to testing the plausibility of proposed geomorphic formation mechanisms. As will be shown, in a model based upon ice conservation, simple expressions for topography and mass balance lead to analytical solutions for the steady state pattern of ice discharge. We assume this ice discharge is a proxy for the long timescale pattern of erosion that stamps the glacial fingerprint over the fluvial morphology. This model allows us to see beyond the limits of simple climates, simple topography, and short timescales inherent to conceptual models by enabling us to explore quantitatively the long timescale pattern of valley erosion while acknowledging both the variability of climate, and the complexity of the valley geometry. Furthermore, the ability to predict the progression of morphology over long timescales permits testing (and refining) of our initial assumptions and simplifications against observations of the real world.

[4] We focus on the longitudinal profiles of glaciated valleys, which depart significantly from their smooth concave-up fluvial counterparts [e.g., *Penck*, 1905; *Sugden and John*, 1976; *MacGregor et al.*, 2000]. Longitudinal profiles are commonly steepened in their headwaters and reduced to lower slopes in the reaches near the terminal moraines that mark the glacial limit (Figures 1 and 2). Some flattened reaches are overdeepened, and are now occupied by either lakes or their sediment-filled equivalent. In addition to this first-order increase in profile concavity, glacial long-valley profiles often show significant steps not seen in fluvial valleys; while some steps clearly coincide with variations in rock resistance, prominent steps in the profile often coincide

[1]Department of Geological Sciences and Institute for Arctic and Alpine Research, University of Colorado, Boulder, Colorado, USA.

[2]Department of Geological Sciences and Cooperative Institute for Research in Environmental Sciences, University of Colorado, Boulder, Colorado, USA.

[3]Institute for Arctic and Alpine Research, University of Colorado, Boulder, Colorado, USA.
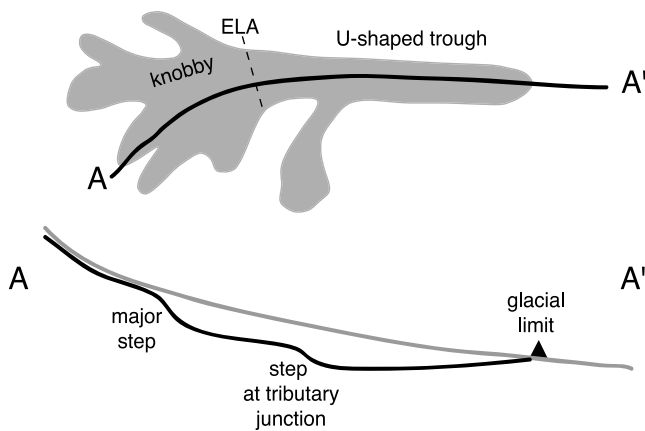
Figure 1. (top) Plan view of glacial footprint showing typical cauliflower-shaped headwaters and tributary junctions. The equilibrium line altitude (ELA) separates the accumulation zone above from the ablation zone below. The bedrock surface in the headwaters is commonly knobby, but that below the main valley junctions is smoother and U shaped in cross section. (bottom) Longitudinal valley profile along A-A' showing initial fluvial profile (gray) and present valley profile (black) showing significant steps corresponding to the coalescence of headwater valleys and to a tributary junction farther down valley.

with tributary junctions [*Penck*, 1905; *MacGregor et al.*, 2000]. Where headwater valleys coalesce, the character of the valley floor commonly changes from a knobby and seemingly disorganized surface to a smooth U-shaped conduit down valley (Figure 2). These two morphologically distinct regions are connected by a step in the longitudinal profile that can be many tens of meters in amplitude (Figures 1 and 2). This feature may be analogous to the "trough head" in valleys draining ice caps, where there appears to be an abrupt transition from ice sheet flow to ice streaming. Discussing this feature, *Sugden and John* [1976, p. 184] suggest that it may reflect a change in "basal ice conditions which determine whether or not the ice slips over the bed."

[5] Present glaciers and paleoglaciers reconstructed from moraine patterns typically have more than half of their surface area at elevations above the equilibrium line altitude, or ELA, which separates the zone of net ice accumulation above from the zone of net ice ablation below. The ratio of accumulation area to total glacier area, AAR ("accumulation area ratio"), is commonly $0.5-0.8$ [*Meier and Post*, 1962], with a strong tendency for the middle of this range, 0.65 [*Porter*, 1975, 1977]. This reflects the hypsometry of the glaciated basin and the dependence of local mass balance (accumulation minus melt) on altitude. In plan view, alpine glaciers display a round-tipped, cauliflower-like branching pattern. Ice occupies a network of headwater valleys that coalesce into a main trunk stream. Part of the natural variability of the AAR may be attributable to the reduction of melt by debris cover that differs among ablation zones. We seek to understand the origin of the observed relatively narrow range of AAR values.

[6] That glaciers leave a signal in the landscape that is fundamentally different from that left by rivers was first

emphasized by *Penck* [1905]. Where rivers carve the landscape, valleys display smooth concave-up longitudinal profiles, a geometry Penck dubbed the normal curve. River discharge monotonically increases downstream as it gathers water from hillslopes and tributaries. A river's ability to erode rock is most often assumed to depend upon both water discharge and slope of the bed. As the water discharge increases downstream, the slope required for incision of
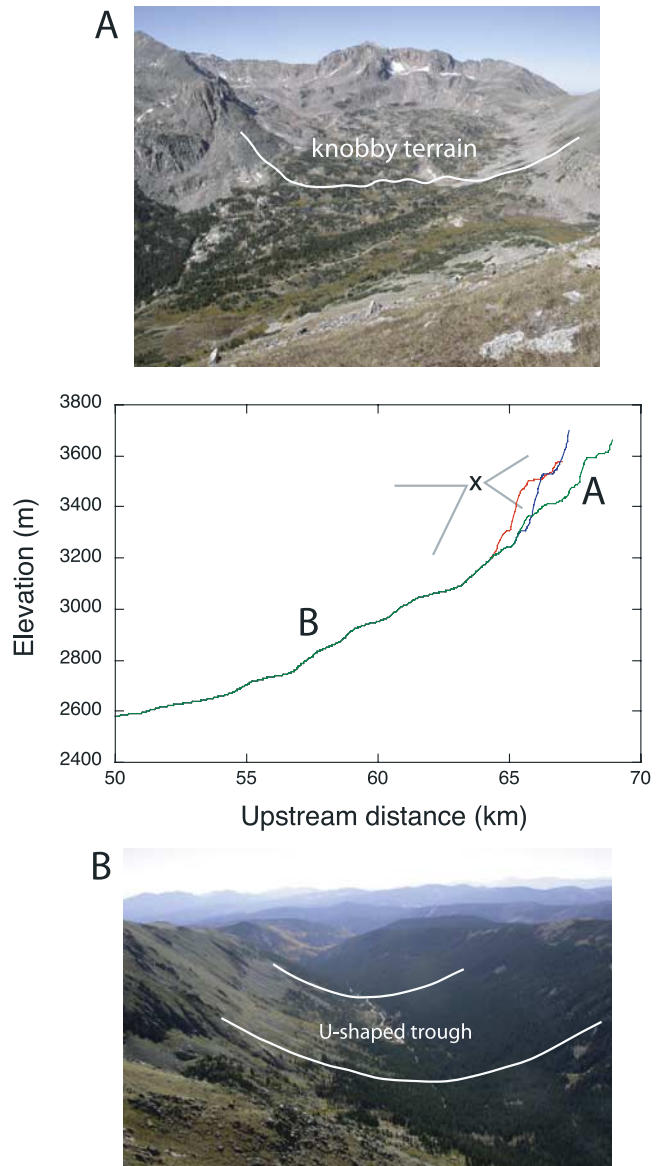

Figure 2. Photos of Fourth of July Valley, Front Range, Colorado, showing longitudinal profile of the glaciated portion of the valley and views (a) up valley and (b) down valley from a vantage point marked as "x" on the profile. Gray angles show approximate view angle for each photograph. Profiles of three headwater tributaries are shown, with major steps as the valleys join. Tributaries farther down valley are not shown; 0 km corresponds to junction with South Platte River on the Great Plains. Cross-valley morphology changes significantly at ~65 km, changing from small-scale bedrock knobs above to smooth and U shaped below.

rock declines. This results in the smooth concave-up longitudinal profile characteristic of fluvial valleys. One key difference between glaciers and rivers is that glaciers end within the alpine landscape, but rivers do not. The discharge of ice does not monotonically increase down valley, but instead increases to a maximum midglacier, and then declines to zero at the glacier terminus. Insofar as ice discharge is a proxy for erosion rate, as is frequently postulated, a fluvial valley that becomes occupied by ice should flatten downstream of an ice discharge maximum and steepened in the headwaters.

[7] This basic explanation for the transformation of a river profile to a glacial one was put forth in a remarkable paper by *Penck* [1905]. He proposed what he called the law of cross sections: the cross section of a glacial trough is adjusted to carry the ice supplied by the mass balance of ice up valley of it. He reasoned that since the surface of the glacier slopes monotonically down valley, the depth and width of the glacial trough must increase to a maximum in midglacier and decay to zero at the terminus. In addition, he concluded that this should flatten and in some instances overdeepen the profile, resulting in the famous lakes that bound the Alps north and south. For the same reasons, Penck argued, there should be steps in glacial valley floors at tributary junctions, as the cross sectional area of the glacier must increase to accommodate the added discharge of ice. A further corollary to the law of cross sections is that because the tributary valleys discharge less ice, they will hang above the trunk stream: while the ice surfaces of trunk and tributary glaciers must smoothly connect, the smaller cross section of the tributary will result in a hang of its channel floor above that of the trunk valley. *Sugden and John* [1976, pp. 182, 183] echoed Penck's principal result, stating that "glacial troughs are equilibrium forms related to the amount of ice discharged" and that "the 'overdeepening' of a glacial trough compared to a river valley is explained by the relative position of the equilibrium line along a trough which usually determines the location of the zone of greatest ice discharge."

[8] Although the transformation from the fluvial V-shaped cross-valley profile to the glacial U shape has been addressed in numerical models [*Harbor et al.*, 1988; *Harbor*, 1992], the evolution of the longitudinal profile has seen less attention. *Oerlemans* [1984] was the first to place this problem in a quantitative context. More recently, using a numerical ice dynamics model with a prescribed mass balance profile, *MacGregor et al.* [2000] reproduced valley floor flattening, explained the hanging of tributary valleys by the discrepancy of long-term ice discharge in the tributary and trunk valleys, and explained steps in the main valley floor by the additional long-term discharge provided by the tributary valley. All of Penck's observations were reproduced. As the numerical simulations reported by *MacGregor et al.* [2000] required time steps equivalent to several days, it was difficult to explore a wide range of mass balance formulations, valley geometries, or specific climate time series with the several hundred thousand year durations needed to investigate longitudinal profile evolution.

[9] Our strategy differs from that of *MacGregor et al.* [2000] in that we calculate ice discharge directly by assuming that the glacier is in steady state with respect to the prescribed climate; we thereby sidestep the short timescale

ice dynamics required to achieve and maintain this condition. Our model can therefore remain analytic. We begin with the simplest case, and then add complexity designed to mimic various aspects of reality with the goal of learning how this additional reality influences basic features of longitudinal valley profiles.

[10] We fully acknowledge that the processes of glacial abrasion, quarrying and subglacial fluvial erosion are responsible for landscape modification by glaciers and that the physics behind their spatial and temporal distribution (1) is probably nonlinearly related to sliding speed, (2) displays coupling among processes, and (3) is linked to the seasonal and even daily evolution of subglacial drainage systems that can incite significant water pressure fluctuations at the bed. As our understanding of these processes and their interactions remains incomplete, and as the timescales over which these vary are many orders of magnitude shorter than those over which valley morphology evolves, we employ a strategy in which a set of simplifying assumptions allow us to explore valley evolution over relevant timescales. The modeling effort of *MacGregor et al.* [2002] suggests that long-term ice discharge over a point is a rough proxy for glacial erosion at that point. In addition, the assembly of sediment yields from glaciated catchments by *Hallet et al.* [1996] suggests that ice discharge can serve as a proxy for erosion rates when averaged over the footprint of the glacier. Both *Penck* [1905] and *Sugden and John* [1976] anticipated these results, arguing that the pattern of erosion was set by the pattern of ice discharge. Here we sidestep the specific erosion processes, and begin by assuming that local specific ice discharge (discharge per unit width) is an adequate proxy for local mean erosion rate over long timescales. Our focus is limited to the roles of climate variability and of valley geometry in setting the long-term pattern of ice discharge, which, if this may be used as a proxy for erosion, transforms longitudinal valley profiles from their original fluvial forms. We seek simple quantitative expressions of the qualitative ideas put forth by *Penck* [1905] and *Sugden and John* [1976].

2. Problem Setup

[11] We require an initial valley profile, and a climate defined by a spatial distribution of mass balance, from which a pattern of ice discharge may be calculated for the steady case.

2.1. Initial Condition

[12] For simplicity we consider a linear valley profile as the initial condition (Figure 3):

$$z = z_{max} - Sx \tag{1}$$

where z is the elevation, S is the slope, x is down-valley distance and $x = 0$ the valley head. Although fluvial profiles are concave up, declining in slope with distance downstream, we start here because two parameters are needed to describe a convex profile, but only one is needed to describe a linear profile.

2.2. Mass Balance Distribution

[13] In order to define the climate the glacier experiences, we seek a distribution of total annual mass balance of ice
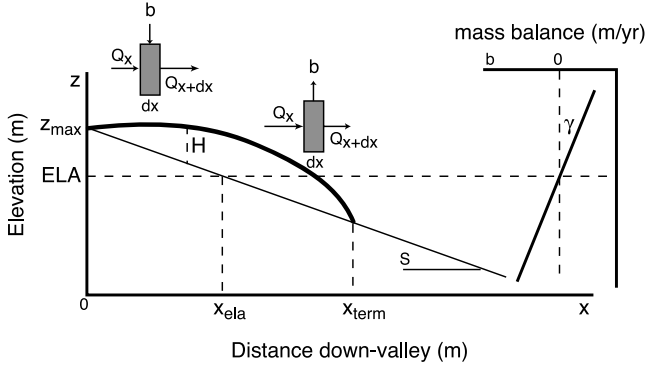
Figure 3. Schematic diagram showing both the linear valley profile and linear mass balance profile employed in our analysis. The steady state model glacier has a thickness profile, $H(x)$, ice discharge pattern, $Q(x)$, and terminus position, x_{term}, that reflect the position of the ELA. Ice columns in accumulation zone, $x < x_{ela}$, and ablation zone, $x > x_{ela}$, are also shown; in steady state the gradient in ice discharge must match the meteorologically set local mass balance.

within the valley. This is the sum of the accumulation by precipitation, and the loss by melt. In many alpine glaciers the distribution of annual mass balance can be described well by a simple function of elevation [e.g., *Meier at el.*, 1971; *Oerlemans and Fortuin*, 1992; *Paterson*, 1994]. Many show an essentially linear increase in the local mass balance, b, with elevation, z, defined by the gradient of balance with elevation, γ, and the elevation at which the balance crosses zero, the equilibrium line altitude, denoted here by z_{ela}:

$$b = \gamma(z - z_{ela}) \qquad (2)$$

Unless otherwise noted, this linear mass balance function was employed.

2.3. Steady State Pattern of Ice Discharge

[14] Given the distribution of annual mass balance with elevation, $b(z)$ in (2), and the initial profile in (1), one can transform $b(z)$ into $b(x)$, the mass balance as a function of distance down valley. Conservation of mass (in this case, of ice) in a representative valley-spanning column of width W requires that the rate of change of ice cross section, HW, include meteorologically driven loss or gain of ice through the top of the column, bW, and the divergence of ice flux through the up-glacier and down-glacier sides of the column (Figure 3). In 1-D, this becomes

$$\frac{\partial(HW)}{\partial t} = bW - \frac{\partial Q}{\partial x}. \qquad (3)$$

For a steady state glacier the left hand side equals zero, and the divergence of ice flux must equal the volume of ice gained or lost through the top of the column:

$$\frac{dQ}{dx} = bW. \qquad (4)$$

The steady state pattern of ice discharge, $Q(x)$ becomes:

$$Q(x) = \int_0^x Wb\,dx. \qquad (5)$$

The location of the glacial terminus lies at the x position where the ice discharge down valley of the ELA vanishes. Using analytical and numerical solutions of this equation, we explore the effects of the climate through $b(x)$ and of valley geometry through $W(x)$.

[15] Here the assumption of steady state requires that we ignore transient response to high frequency climate variations. Typical response times of valley glaciers to climate change are on the order of 100 years [*Johannesson et al.*, 1989; *Harrison et al.*, 2001]. Our focus is on evolution of longitudinal valley profiles due to mass balance profiles that vary on timescales of thousands to hundreds of thousands of years. Thus this assumption that the glacier is in steady state with the climate forcing is reasonable.

2.4. Accumulation Area Ratio

[16] Armed with the geometry of the valley, represented by $W(x)$, the mass balance profile, represented by $b(x)$ from which the x position of the ELA is known, and the pattern of ice discharge from which the glacial terminus position, x_{term}, is assessed, we can calculate the accumulation area ratio:

$$AAR = \frac{\displaystyle\int_0^{x_{ELA}} W\,dx}{\displaystyle\int_0^{x_{term}} W\,dx} \qquad (6)$$

in which the numerator is the area of the glacier above the ELA, and the denominator is the total area of the glacier.

3. Steady Climate, Simple Valley of Uniform Width

[17] We first consider the pattern of ice discharge in a valley with uniform width, $W = W_o$, a uniform slope $= S$, and a climate characterized by a linear mass balance profile captured in (1) (Figure 4). Integrating (5) yields the ice discharge:

$$Q = W_o\gamma\{(z_{max} - z_{ela})x - (Sx^2/2)\} \qquad (7)$$

This is parabolic, with a peak at the x position corresponding to the ELA ($x_{ela} = (z_{max} - z_{ela})/S$). The terminus position x_{term} may be calculated simply by solving for where the ice discharge declines to 0:

$$x_{term} = \frac{2(z_{max} - z_{ela})}{S} \qquad (8)$$

The down-valley location of the terminus is twice the distance of the x position of the ELA (Figure 5); the AAR is therefore 0.5 and the flux of ice Q is symmetric about the ELA.
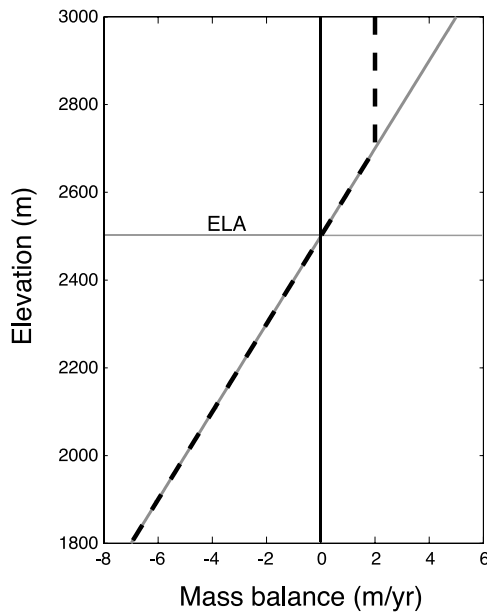
Figure 4. Mass balance profiles, $b(z)$, each with ELA = 2500 m, linear profile with gradient $\gamma = 0.01$ (gray), and mass balance profile with a maximum for elevations above 2700 m (dashed).

[18] As argued in the section 1, ice discharge has been argued to be a proxy for the rate of glacial erosion. If this is correct, the maximum erosion rate should occur at the ELA (Figure 5). Down valley of this maximum, the erosion rate should decline rapidly to zero at the terminus, beyond which erosion would be dictated instead by fluvial processes. The glacier would take a parabolic divot out of the original longitudinal profile. The first-order effect is therefore valley floor flattening down valley of the x position of the ELA through time, and valley floor steepening up valley of it. This is indeed the essential signature of valleys once occupied by glaciers, and reproduces the principal result from the numerical glacial modeling presented by *MacGregor et al.* [2000]. As shown here, this is an extremely robust result, unrelated to the glacier mechanics, relying only on conservation of ice under the most general conditions of climate and valley geometry. These simple assumptions and the resulting calculations, however, fail to reproduce at least two fundamental observations about real glacial valleys. First, although the valley near the headwaters is steep, the commonly observed step in the valley profile is not reproduced. Second, the distribution of ice represented by the analytical result is symmetrical about the ELA; as much area lies above as below it, and the calculated accumulation area ratio, AAR = 0.5, not the commonly observed 0.65. In order to address these issues, we add elements of reality to this model one at a time.

[19] 1. We first explore the effect of a more realistic mass balance profile that incorporates a maximum balance, rather than a linear increase, at high elevations.

[20] 2. Next we explore the impacts of variability in the climate, assuming various forms for the probability density functions (pdfs) of the ELA.

[21] 3. We then acknowledge that the effective width of real glacially occupied valleys varies dramatically in the

headwaters, i.e., $W = f(x)$ and cannot be assumed to be a constant, $W = W_o$.

[22] 4. Finally, we explore briefly different erosion rules, including nonlinear dependence on discharge per unit width.

[23] As we show below, although each of these steps takes us closer to real glaciers and real glacial valleys, the simple analytic result given by (7) and (8) and shown by the black line in Figure 5 captures the essence of the glacial valley profiles.

4. Effect of Mass Balance Profile Shape

[24] It is often observed [e.g., *Meier et al.*, 1971; *Oerlemans and Fortuin*, 1992] that the gradient in mass balance profile $\gamma = db(z)/dz$ is lower at the highest elevations than along much of the glacier [e.g., *Furbish and Andrews*, 1984]. To consider an extreme form of this elevation dependence, we assume that above some elevation z_m the mass balance is constant (dashed line in Figure 4):

$$b = b_{max}; z > z_m$$
$$b = \gamma(z - z_{ela}); z < z_m \tag{9}$$

The steady state ice discharge, again from (5), becomes

$$Q = W_o b_{max} x; \quad x < x_m$$
$$Q = W_o b_{max} x_m + W_o \gamma \{(z_{max} - z_{ela})(x - x_m) - (S(x^2 - x_m^2)/2)\};$$
$$x >= x_m \tag{10}$$

where x_m is the down-valley position at which the mass balance first drops below b_{max} (the x position of z_m),

$$x_m = \frac{z_{max} - \left(\frac{b_{max}}{\gamma} + z_{ela}\right)}{S}. \tag{11}$$

For this case, ice discharge increases linearly down valley in the headwaters as the contributing area increases before
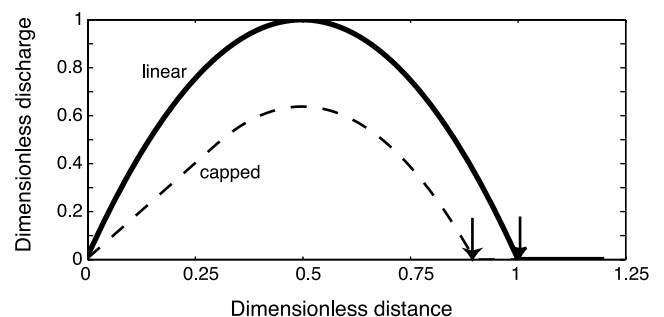

Figure 5. Ice discharge patterns for two cases, both in simple linear valley with uniform width, normalized using the terminus position, $2((z_{max} - z_{ela})/S$, and maximum ice discharge at the ELA for the linear case. Solid line, linear $b(z)$ and no cap; dashed line, same gradient and ELA but capped (as shown in Figure 4). Both peak at the same location in the valley, at the down-valley position of the ELA. Terminus positions (arrows) reflect where the ice discharge goes to zero.

becoming parabolic at $x \geq x_m$ (dashed line in Figure 5). Because less ice accumulates than for the case represented by (7), the terminus position extends a shorter distance down valley, and the peak discharge is reduced. The asymmetry in the mass balance is also reflected in accumulation area ratio. In the case of a uniform valley width, equation 6 becomes $AAR = x_{ela}/x_{term}$. The AAR is now greater than 0.5, and increases as the elevation band experiencing the capped mass balance expands. For the case illustrated by the dashed line in Figure 5, $AAR = 0.56$.

5. Variability of Climate

[25] Climate varies during erosion of large-scale glacial features, causing advances and retreats of glaciers. This can be captured as variability in the ELA. As we are interested only in the long-term integrated pattern of ice discharge and erosion, we avoid specifying a history of the ELA, but turn instead to its probability distribution. We consider three simple probability distributions of ELAs. We explore first the mathematically simplest distribution, a uniform probability of finding the ELA at any altitude between E_{min} and E_{max}. We then explore the effect of a sinusoidally varying ELA, and finally a Gaussian distribution, which is inspired by the distribution of $\delta^{18}O$ in the Plio-Pleistocene deep-sea record [e.g., *Zachos et al.*, 2001].

[26] In all cases, we seek the spatial pattern of long-term average ice discharge, represented by

$$\overline{Q}(x) = \int_E Q(x,E)p(E)dE \tag{12}$$

where $p(E)$ is the probability density function (pdf) of the ELA, E, and $Q(x,E)$ is the instantaneous pattern of ice discharge corresponding to a given ELA, as captured in (7).

5.1. Uniform Distribution of ELAs

[27] A uniform distribution of ELAs can be described by the pdf

$$p(E) = \frac{1}{E_{max} - E_{min}} \tag{13}$$

There are two parts of the profile that must be treated separately (Figure 6), the upper part of the valley always occupied by a glacier ($x < x_{min}$), and the lower part where for some of the time no glacier is present ($x > x_{min}$). For the former region, the integral becomes:

$$\overline{Q} = \int_0^\infty Q(x,E)p(E)dE$$

$$= \frac{\gamma W_o}{E_{max} - E_{min}} \int_{E\,min}^{E\,max} \left[(z_{max} - E)x - \frac{Sx^2}{2} \right] dE \quad \text{for } x < x_{min} \tag{14}$$

The solution is

$$\overline{Q}(x, x < x_{min}) = \frac{\gamma W_o}{\Delta E} \left[x^2 \left(-\frac{S\Delta E}{2} \right) + x \left(z_m \Delta E + \frac{E_{min}^2}{2} - \frac{E_{max}^2}{2} \right) \right] \tag{15}$$
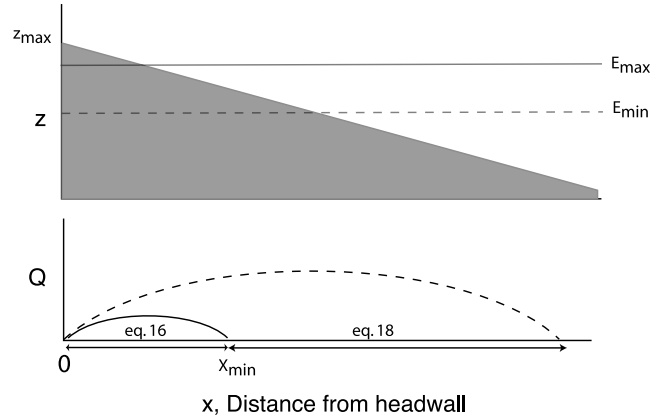

Figure 6. Schematic illustrating the two domains in the solution for ice discharge with ELAs uniformly distributed between E_{min} and E_{max}. Minimum and maximum size glaciers corresponding to highest and lowest ELA are shown as solid and dashed lines. For all locations between the headwall at $x = 0$ and the terminus of the minimum length glacier, x_{min}, there is always a glacier, and equation (16) applies. For all locations beyond x_{min}, some fraction of the time is spent with no glacier, and equation (18) applies.

The solution appropriately collapses to the steady climate case (equation (7)) when $\Delta E = E_{max} - E_{min}$ vanishes.

[28] Down valley of the position x_{min}, calculation of the long-term discharge requires acknowledging that the minimum glacier extends only to x_{min} (Figure 6). This is accommodated by changing the maximum limit of integration to the ELA that would generate a glacier terminating at the position x: $E_c = z_{max} - (xS/2)$. Higher ELAs do not contribute ice past this position:

$$\overline{Q}(x) = \int_0^\infty Q(x,E)p(E)dE$$

$$= \frac{\gamma W_o}{E_{max} - E_{min}} \int_{E_{min}}^{z_{max} - xS/2} \left[(z_{max} - E)x - \frac{Sx^2}{2} \right] dE \tag{16}$$

Evaluation of this integral yields a third-order polynomial equation in x:

$$\overline{Q}(x, x \geq x_{min}) = \frac{\gamma W_o}{\Delta E} \left[x^3 \left(\frac{S^2}{8} \right) - x^2 \frac{S}{2}(z_{max} - E_{min}) \right.$$
$$\left. + x \frac{1}{2}(z_{max} - E_{min})^2 \right] \tag{17}$$

A plot of the solution given by (15) and (17) (Figure 7) shows that the essence of the ice discharge pattern derived for a steady climate remains intact. Assuming erosion increases with ice discharge, climate variability results in a smoothing of the transition to the fluvial profile beyond the maximum glacier terminus. The symmetry of the pattern is now broken, however, as larger glaciers corresponding to ELAs below the mean ELA contribute more to the long-
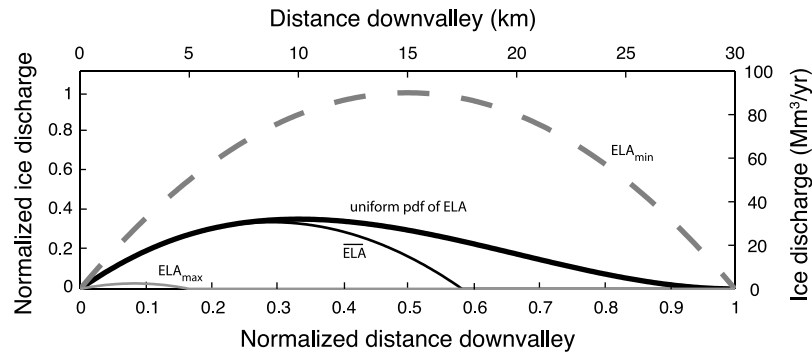
Figure 7. Analytic solution for ice discharge patterns resulting from steady state glaciers driven by a simple mass balance function, in a linear valley profile, and a uniform distribution of ELAs. Maximum and minimum glaciers corresponding to minimum and maximum ELAs, respectively, are shown along with the glacier discharge expected from the average ELA and a long-term average resulting from a uniform distribution of ELAs between maximum and minimum. The symmetry is broken when a distribution of ELAs is permitted. Maximum discharge occurs down valley from that corresponding to the mean climate, at roughly one third of the glacial limit (the maximum terminus position), and smoothly tapers to zero discharge there. Distance and ice discharge are normalized using glacier length and ice discharge associated with the lowest ELA.

term average ice flux and erosion than do their smaller, higher ELA counterparts.

[29] In the case depicted in Figure 7, for which the ELA always lies below the peak elevation of the valley, the location of the maximum ice discharge roughly coincides with that of the glacier corresponding to the mean ELA, but we cannot expect this to be the general case in the face of variable climate. What happens to the pattern we have identified when some portion of the ELA distribution lies above the peak of the topography, i.e., if there are times in the history of the valley in which glaciers do not exist? This effectively truncates the distribution of ELAs at z_{max}. Consider the case in which for part of the time the ELA lies above the peak of the topography. Glaciers still flick their tongues down the valley during excursions of the ELA below z_{max}. Correspondingly, as the distribution of ELAs begins to exceed the maximum elevation of the valley, equation 18 applies along the entire valley, because $x_{min} = 0$. We can then evaluate formally the location of the peak ice discharge by taking $dQ/dx = 0$ in equation 18. This yields the prediction that when the distribution of ELAs is uniform, and some portion of the distribution lies above the peak elevation of the valley, the peak discharge and hence the peak erosion ought to occur at $x = \frac{2}{3}\frac{(z_{max}-E_{min})}{S}$. This is two thirds of the distance from the divide to the location of the peak discharge associated with the glacier corresponding to the lowest ELA, and hence one third of the distance from the divide to the terminus of the longest glacier. One can see in Figure 7 that this is approximately the case also when the maximum ELA lies below z_{max}, indicating that the discharge contribution from these small glaciers (high ELAs) is negligible.

5.2. Harmonically Varying ELA

[30] For a harmonically varying ELA,

$$E = \overline{E} + \Delta E \sin(\omega t)) \qquad (18)$$

where $\overline{E}$ is the mean ELA and ΔE the (half) amplitude of its variability. The probability density function of ELA is:

$$p(E) = \frac{1}{\sqrt{\Delta E^2 - \left(E - \overline{E}\right)^2}}; \quad \left|E - \overline{E}\right| < \Delta E \qquad (19)$$

and is zero outside of these bounds (Figure 8). The probability distribution reaches its maximum for ELAs at either its maximum or minimum height, where it changes
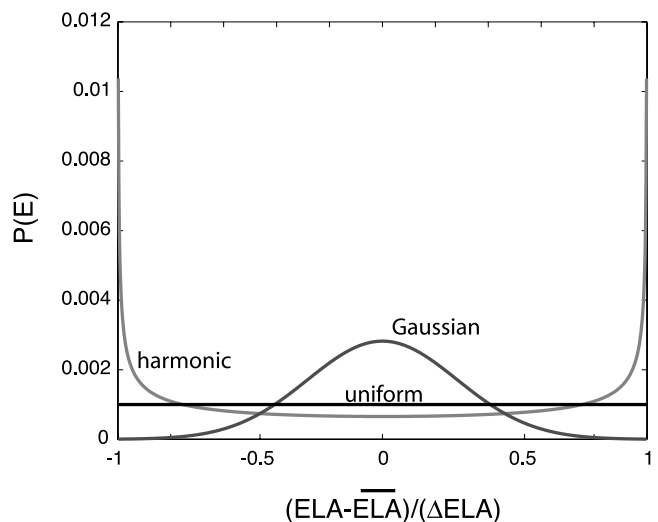

Figure 8. Probability density functions (pdfs) of ELA used in the analytic solutions for ice discharge. ELA is nondimensionalized with the difference between maximum and mean ELA for uniform and harmonic distributions and with 2σ for Gaussian distribution. The harmonic history yields a pdf that peaks at the minimum and maximum ELA, while a history that is normally distributed about the mean spends the least time at the minimum and maximum ELA.
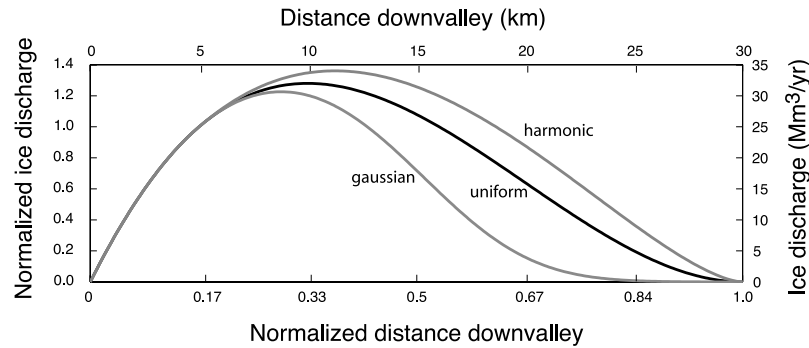
Figure 9. Analytic solutions for long-term average discharge of ice when the ELA is distributed using three different pdfs, each with the same mean ELA (=3400 m; ΔE = 400 m). Nondimensional axes were normalized with maximum glacial extent, and maximum discharge is associated with the mean ELA position for the case of uniform distribution of ELAs.

slowly; the ELA lies near its average value for only short intervals, because it crosses that level quickly. The sinusoidal case promotes more erosion down valley than in the uniform case (Figure 9), because the large glaciers corresponding to the lowest ELA spend more time near their maximum extent than in the case of uniformly distributed ELAs (Figure 8).

[31] Although we have focused on the pdf of the ELA, in Appendix A we cast the problem in the time domain and determine the expected pattern of erosion over a sinusoidal history. The two approaches yield the same result.

5.3. Gaussian Distribution of ELAs

[32] One might expect that the most appropriate distribution of ELA is normally distributed around a mean:

$$p(E) = \frac{2}{\sqrt{\pi}} e^{-\left((E-\overline{E})/\sigma\right)^2} \qquad (20)$$

For example, the pdf of $\delta^{18}O$ measured in benthic foraminifera since 1.5 Ma [Zachos et al., 2001], a surrogate for the volume of ice stored on land, is roughly normally distributed (Figure 10). Again, the results are not very different from those for the uniform distribution. The integrated ice discharge falls off more rapidly with distance down valley than in either the uniform or sinusoidal case, as

the probability of the lower ELAs, corresponding to longer glaciers, declines (Figure 9).

[33] In summary, the form of $p(E)$, representing a statistical summary of climate variability, does not change the essence of the spatial pattern of long-term ice discharge that we discussed above. When variability of climate is incorporated, the pattern of long-term ice discharge and hence the expected pattern of erosion becomes asymmetric. The pattern of erosion is most sensitive to the structure of the probability density function near the lowest ELA. Variability in ELA leads to a gradual, not abrupt, decrease in long-term ice discharge toward zero at the glacial limit. In all cases depicted in Figure 9 the asymmetry is such that the peak long-term discharge occurs at roughly 1/3 of the distance to the glacial limit. We showed above that this is formally the case when $p(E)$ is uniform, and some portion of this distribution lies above the head of the valley. Further numerical exploration of the uniform $p(E)$ case reveals that the ratio of down-valley distance to erosion maximum to the distance to the glacial limit declines from about 0.4 when the full distribution of the ELA lies below the topography, to 0.33 as the ELA rises. The ratio varies even less, remaining about 0.4, for the sinusoidal distribution. We note that this constitutes a prediction: from valley profiles in which rock susceptibility to erosion is uniform, and in which valley geometry is simple, one could evaluate whether the erosion
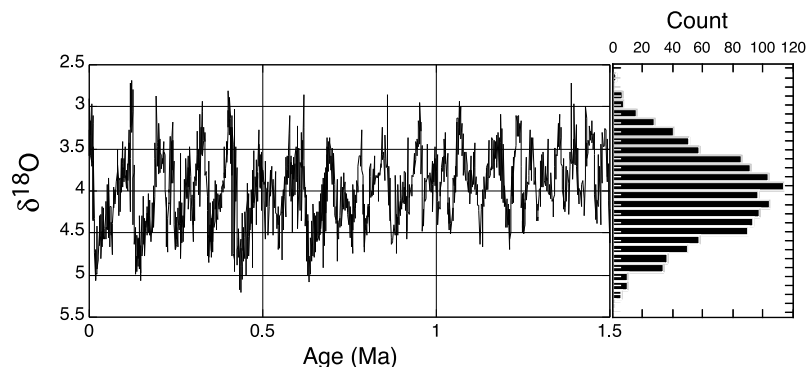

Figure 10. Marine isotopic record for last 1.5 Ma [after Zachos et al., 2001] and a histogram of it. The distribution is roughly symmetric and appears to be normally distributed.
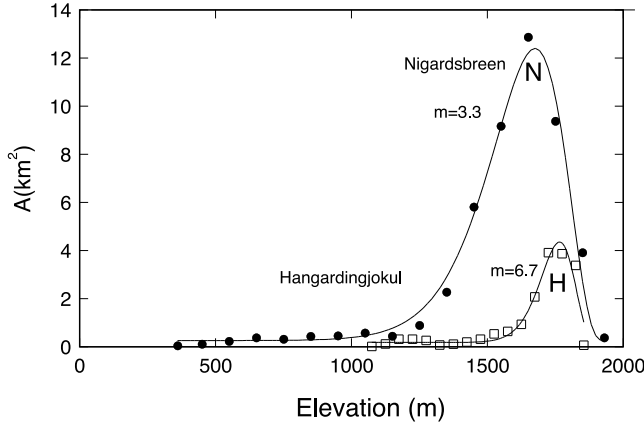
Figure 11. Area distribution with elevation on two well-studied Norwegian glaciers (N, Nigardsbreen; H, Harangingjokul). As the area is reported for fixed intervals of elevation (data from *Elvehoy et al.* [1997]), the pattern could be translated into one of effective glacier width versus elevation. The best fit curves for the gamma distribution employed in this paper are shown as well, with the power, *m*, indicated.

maximum occurs roughly 1/3 the way from the headwall to the terminal moraine at the glacial limit.

6. Effect of Nonuniform Valley Width

[34] Despite a low vertical gradient in accumulation rate at high elevations, ice can accumulate faster there than we have assumed because the fraction of area covered by ice is maximum near the head of a valley glacier system. All drainage basins are composed of a network of valleys that branch up valley. The occupation of such a network by glaciers results in a round-edged cauliflower-like plan view of the glacier footprint. The distribution of effective valley widths as a function of elevation is generally reported in terms of a hypsometric curve, the cumulative distribution of the area occupied by glaciers above a given elevation. For our purposes, we need instead the dependence of valley width on elevation, $W(z)$, which we then transform into a function of distance down valley through knowledge of $z(x)$. As shown by the area distributions of Norwegian glaciers (Figure 11), which can be translated into width distributions with a knowledge of the elevation increment used, a general function that can represent the width distribution is:

$$W = W_o \left(1 + \varphi \left(\frac{x}{x_*} \right)^m e^{-\frac{x}{x_*}} \right). \quad (21)$$

For these glacial valleys, the exponent *m* is near 4, and the length scale *x** is on the order of 1 km to a few kilometers. Here the constant φ determines the importance of the tributary widening in the headwaters, *x** determines the down-valley position of the maximum width and tapering of width beyond it, and *m* controls the shape of the upstream expansion of width. This pattern sums a uniform width W_o, with a general form of the gamma function, $(x/x_*)^m e^{-(x/x_*)}$, and collapses to the uniform width case discussed above if we take $\varphi = 0$.

[35] Incorporating the width function represented by (21) into the calculation of the expected steady state ice discharge for a linear valley with the linear mass balance profile from (5) yields

$$Q = \gamma \int_0^x [(z_{\max} - Sx) - z_{ela}] \left[W_o + \varphi W_o \left(x/x_* \right)^m e^{-\left(x/x_* \right)} \right] dx \quad (22)$$

This can be evaluated analytically:

$$Q = Q_u + C + \frac{\gamma \varphi W_o (z_{\max} - z_{ela})}{x_*^m} e^{-x/x_*} \sum_{r=0}^m (-1)^r$$
$$\cdot \frac{m! x^{m-r}}{(m-r)! \left(-1/x_* \right)^{r+1}} - \frac{S \gamma \varphi W_o}{x_*^m} e^{-x/x_*} \sum_{r=0}^{m+1} (-1)^r$$
$$\cdot \frac{(m+1)! x^{m+1-r}}{(m+1-r)! \left(-1/x_* \right)^{r+1}} \quad (23)$$

where Q_u is the solution for the uniform width case, equation (7). The requirement that the ice discharge $Q = 0$ at the top of the valley (at $x = 0$) sets the constant of integration:

$$C = \varphi W_o \gamma \left[(z_{\max} - z_{ela}) x_* m! + S x_*^2 (m+1)! \right]. \quad (24)$$

[36] The resulting pattern of ice discharge (Figure 12) increases rapidly in the headwaters, as it includes ice from an increasingly wider accumulation area. For any given mass balance distribution with elevation, the peak discharge is therefore much greater than that of a valley with uniform
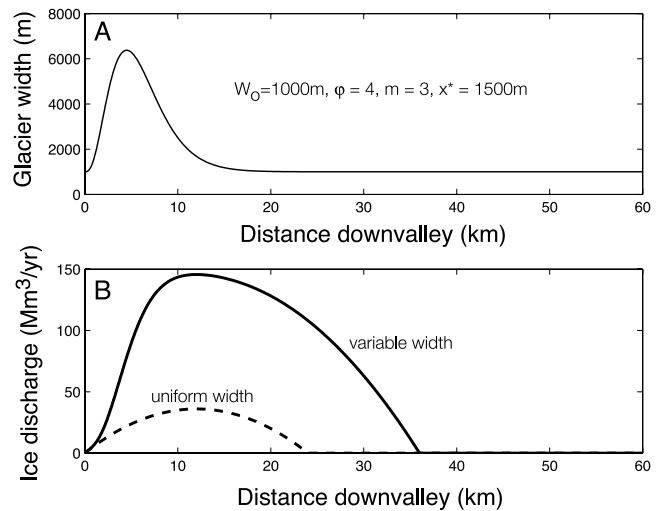

Figure 12. Effect of variation in glacier width with distance down valley. (a) Profile of valley width, following offset gamma function. (b) Ice discharge in variable width valley (thick line) contrasted with uniform width case. The added width requires greater discharge at all down-valley locations. Peak discharge occurs at roughly the same elevation (the ELA). Beyond the location at which the width becomes uniform the discharge follows the expected parabolic pattern.
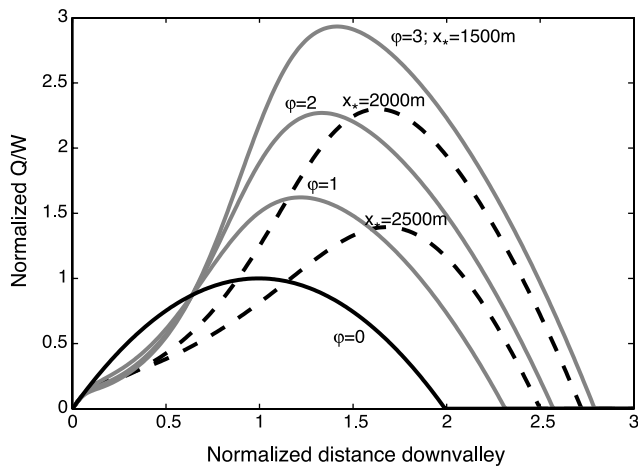
Figure 13. Dimensionless discharge per unit width as a function of dimensionless distance down valley for various valley width profiles. Solid lines show that for a given $x_* = 1500$ m, as φ increases from 0 (uniform width case), the valley asymmetry increases, and maximum specific discharge both increases and reaches its maximum at increasing distances down valley. Dashed lines show that for a given $\varphi = 3$, as the length scale setting the down-valley dimension of the bulge in width, x_*, increases, the maximum discharge declines but moves farther down valley. Distance and ice discharge are normalized with respect to terminus position and maximum ice discharge associated with uniform width valley.

width W_o. The pattern of ice discharge returns to the parabolic form downstream of the bulge in glacier width (i.e., once the valley returns to a uniform width). Because of the greater flux of ice past the ELA, the glacier extends a much greater distance down valley than does a glacier in a valley without multiple headwater tributaries.

[37] To explore the effect of valley geometry on the expected glacial erosion pattern, we note that ice discharge per unit width, Q/W, or "specific discharge" (Figure 13) is more likely to reflect the erosion rate than is ice discharge, as it acknowledges that ice must both speed up and thicken to maintain the same discharge in a narrow valley. Although ice speed is undoubtedly a yet better proxy for erosion rate, calculation of mean ice speed would require a model for ice thickness, as we discuss below. As φ increases from 0 (uniform width case), the down-valley width asymmetry increases, and maximum specific discharge both increases and reaches its maximum at increasing distances down valley (Figure 13). For a given φ, the location of the maximum specific discharge moves farther down valley as x_* increases, reflecting the fact that x_* scales the location of the convergence of headwater valleys (Figure 13). However, the convergence weakens as x_* increases, reducing the peak in specific discharge. In short, the details of valley geometry play an important role in setting the details of the pattern in specific ice discharge. The locus of maximum erosion can be shifted significantly down valley of the x position of the ELA.

[38] A step in the valley profile near the headwaters (Figure 12 or Figure 14) emerges, if erosion is proportional either to specific discharge (Figures 12a and 14a) or to its

square (Figures 12b and 14b). The location of the step is tied to the valley geometry. The step begins immediately down valley of the maximum width (Figure 12), as high ice discharge is made to funnel through a narrowing valley. The step is accentuated if the erosion rule varies as a power of specific discharge. Erosion is significantly reduced in the headwaters above the step, where the large valley width allows specific discharge to be low.

7. A Simulation That Considers Realistic Conditions

[39] For comparison with real glacial valley profiles, we include in a numerical simulation that includes all of the elements of reality that we have addressed singly in previous cases (Figures 15 and 16). We assume an initially linear valley, but we include a nonuniform valley width distribution (Figure 12), a mass balance profile that at any time is linear until a cap at 2 m/yr is reached (Figure 4), and an ELA normally distributed about a mean elevation of 3400 m, with standard deviation of 600 m. The patterns of ice discharge for any given ELA are similar to that depicted in Figure 12, except that the discharge is reduced in the headwaters, resulting in a smaller peak discharge due to the capped mass balance profile. As in the case with a Gaussian distribution of ELA (Figure 9), the long-term mean ice discharge (or specific discharge) is tapered near the glacial limit reflecting the lower probability of ELAs at lower limit of the distribution. In the headwaters, the taper, which can be seen in the pattern of ice discharge for all glaciers (Figure 15a), reflects the structure of the valley width distribution. The resulting long-valley profile, with a major step in the headwaters, flattening of the valley floor near the mean ELA, and tapering of the profile into the fluvial profile near the glacial limit, contains all of the features of the simpler cases.

[40] The dependences of glacial characteristics of length, area, and accumulation area ratio (AAR) on the ELA
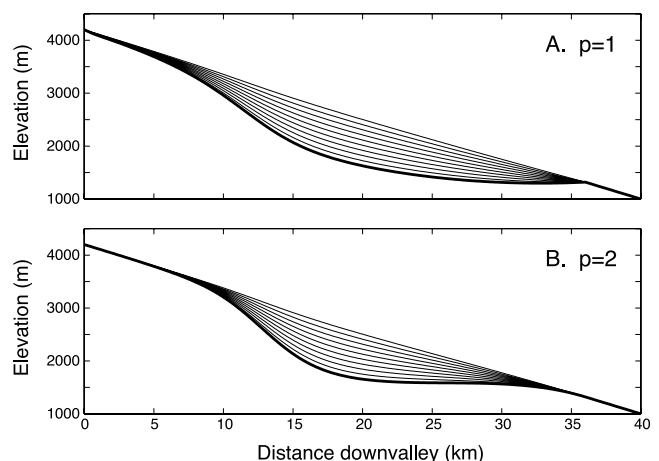

Figure 14. Expected valley profile evolution for steady climate, using valley width defined by x* = 1500 m and ϕ = 3. (a) Erosion rate proportional to ice discharge per unit width to the power p = 1 and (b) erosion rate proportional to Q/W to the power p = 2. Individual lines represent snapshots of valley profile at evenly spaced intervals.
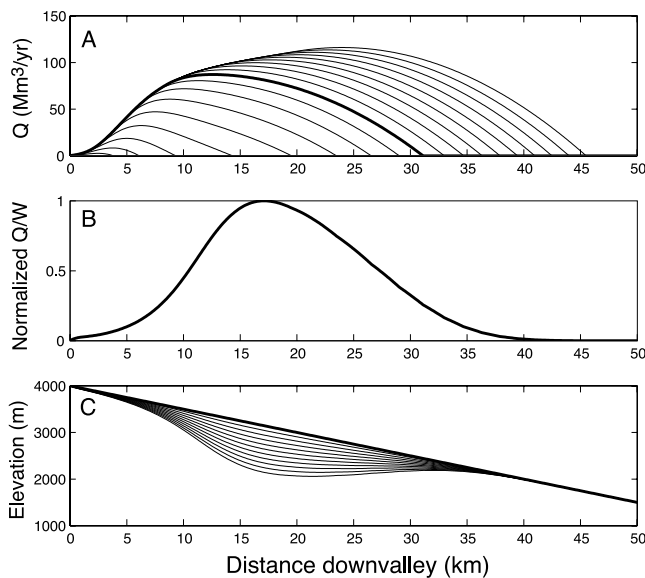
Figure 15. Calculations of ice discharge and resulting patterns of erosion for a case in which climate is characterized by a mass balance capped at 2 m/yr (see Figure 4), a Gaussian distribution of ELA with mean of 3400 m, and a valley in which width varies as in Figure 12. (a) Ice discharge for 20 ELAs ranging from 2800 to 4000 m ($=z_{max}$). Discharge associated with the mean ELA is shown by a thick line. (b) Long-term mean ice discharge per unit width, normalized with its maximum value. (c) Erosion of long-valley profile in 10 time intervals using the long-term mean Q/W as a proxy for erosion rate. Note strong step in profile down valley of peak in valley width (at 5 km, see Figure 12), flattening of valley floor, and smooth tapering of valley into initial fluvial profile.

(Figure 16) vary nearly linearly for ELAs well below the rapid decrease in width, but are strongly nonlinear when the ELA is high in the valley and the width varies markedly with elevation. In these simulations, for all ELAs that produce glaciers more than a few kilometers in length, the AAR varies between 0.60 and 0.73.

8. Discussion and Conclusions

[41] We have shown how the mass balance profile, and the valley geometry conspire to set the pattern of glacial modification of a valley, assuming that erosion depends simply on the flux of ice past a point on the bed. The most fundamental effect is revealed in the first and simplest case: because the pattern of ice discharge reaches a maximum at the ELA, the pattern of erosion ought to mimic this. *Sugden and John* [1976] suggested that glacial valleys should be most deeply eroded near the long-term mean ELA. Although many of the cases we have considered appear to support this conclusion, this cannot hold when the mean ELA lies above the tip of the topography. The mean ELA worsens as a predictor of the erosion maximum as more of the distribution of ELAs rises above the topography. What appears to be more robust in all cases is that the erosion maximum occurs at roughly 1/3 of the distance from the valley head to the glacial limit, the terminus of that glacier corresponding to the lowest ELA. Up valley of this maximum in erosion the valley profile will be steepened

and down valley the valley floor will be flattened as the long-term integrated ice discharge declines in both directions. Although details of the mass balance profile modify the expected erosion pattern, assuming that erosion varies with the flux of ice, these details do not alter the general result. Incorporation of a variable climate acts to smooth the pattern, but does not alter it in a fundamental way. Glacial erosion should smoothly approach zero at the glacial limit, with the details of this pattern set by the probability distribution of ELAs.

[42] The coalescence of glacial tributaries in the headwaters of glacial valleys creates the most marked deviations from the simple pattern outlined above. Inspection of map view shapes of glaciers, and compilations of the distribution of area with elevation, show that glaciers display a prominent bulge in accumulation area at high elevations, where short headwater glacial valleys coalesce to form a single long valley. This pattern is largely inherited from the branching pattern of fluvial networks. Ice discharge per unit width increases markedly where the valleys coalesce to become the trunk glacier. If specific discharge is a proxy for glacial erosion, then this pattern will create a step in the valley that coincides with the tributary confluence, as argued long ago by *Penck* [1905]. It may be argued that this effect could also explain the prominent break in the morphology of some glacial valley floors, in which poorly organized knobby bedrock valley floors give way to organized, classic U-shaped troughs down valley of the convergence of ice (Figure 2). One could potentially test this
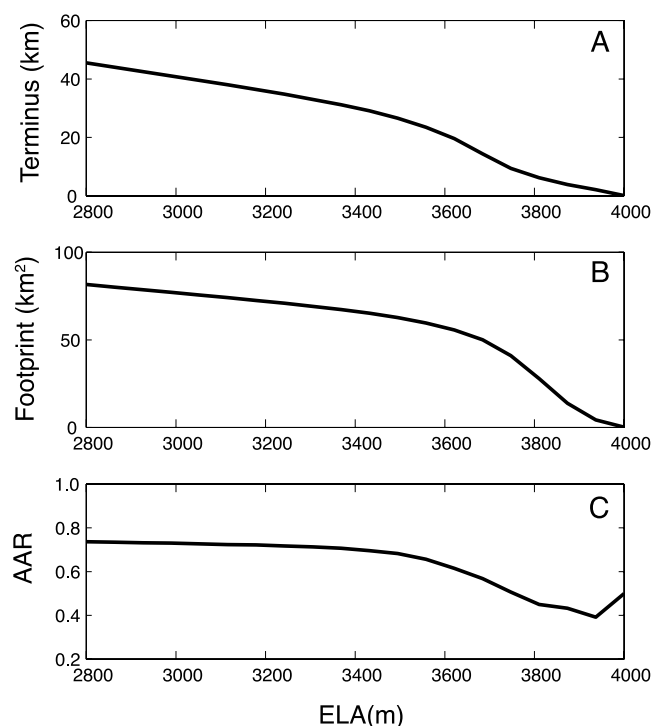

Figure 16. Dependence of glacial characteristics on ELA for case described in Figure 15. (a) Terminus position, (b) glacial footprint, and (c) AAR. Note nonlinear relationships, with strong increases in all features as ELA drops below elevation of maximum valley width. Most AAR values lie between 0.5 and 0.75.

notion by placing limits on the total erosion accomplished in the last glacial cycle using cosmogenic radionuclide concentrations in the bedrock valley floor. We would predict that in the knobby headwater valley floor the cosmogenic radionuclide concentrations accumulated in prior interglacials may not have been fully erased by erosion during the last glacial cycle (requiring roughly 3–5 m of erosion), but polished outcrops in the U-shaped trough may have been.

[43] The valley geometry is largely responsible for setting the accumulation area ratio, or AAR associated with a glacier at any point in time. The observed AAR range of 0.5–0.8 is mostly a reflection of valley geometry. In simple cases of uniform width and linear mass balance profile, accumulation will mirror ablation and the AAR is inevitably 0.5; the pattern of ice discharge is parabolic and hence symmetrical about the ELA. Altering the mass balance profile by reducing the accumulation with a cap at high elevations results in an AAR above 0.5, as the discharge declines more rapidly below the ELA than it rises in the headwaters. This effect grows for lower ELAs because the area experiencing a maximum positive balance independent of elevation increases (dashed line in Figure 4). However, the effect does not yield an AAR much above 0.55. The observed AAR range of 0.5 to 0.8 instead largely reflects the distribution of valley widths with elevation. We have shown in Figure 16 that AAR $\approx$ 0.7 ought to be common in valleys with significant bulges in width distributions at high elevations. As ablation occurs at the ice surface, concentration of ice into a thick, narrow trunk stream in the ablation zone allows it to access lower elevations with more negative mass balances. As the accumulation area times the area average accumulation must equal the ablation area times the average ablation, the highly negative average ablation must be balanced by an increased area of accumulation, resulting in a higher AAR, a result formalized by *Furbish and Andrews* [1984]. Differences in the details of the width distribution result in differences in the maximum AAR. A more comprehensive analysis of the controls on the AAR would require relaxing our linear initial valley profile. Finally, we acknowledge that some of the natural variability of the AAR from one to another glacier is attributable to the reduction of melt by debris cover that differs among ablation zones. This debris cover reflects both the rate of production of debris from valley walls in the headwaters, and down-valley widening and coalescence of medial moraines from tributary glaciers [e.g., *Anderson*, 2000].

[44] We have assumed throughout our analysis that the glacier remains in steady state, allowing us to balance meteorologically driven mass balance with spatial gradients in ice discharge. We therefore cannot treat variations of glaciers that are shorter than typical response times of hundreds of years. As long as the patterns of ice discharge do not differ greatly during the transient phases of advance and retreat that we cannot mimic, our approach should still be valid.

[45] We acknowledge that ice discharge per unit valley width is only a crude proxy for the physics of glacial erosion. In reality, both abrasion and quarrying are tied to the sliding speed of ice. As ice discharge is $Q = WH\overline{U}$, where $\overline{U}$ is the mean ice speed (the sum of sliding and the vertically averaged ice deformation speed), it is clear that Q/W still contains both ice thickness and ice speed. As long

as ice thickness does not vary as rapidly as ice width, then variations in Q/W could well mimic ice speed. To the degree that variations in ice speed are then accommodated by variations in sliding speed, Q/W will mimic sliding speed. Clearly, this is a tenuous set of approximations. We are heartened by the degree to which patterns of glacial erosion calculated using a model that explicitly accounts for ice deformation and sliding [*MacGregor et al.*, 2000] mimic those simulated here. Further exploration of the problem awaits better knowledge of how to parameterize both the sliding speed distribution beneath a glacier, and how the erosion processes are tied to this sliding.

[46] Although the strong dependence of glacial length and area on ELA (Figure 16) may at first seem academic, we emphasize that this analysis quantifies the strong coupling between glaciers and the rivers downstream, into which the sediment derived from glacial erosion is delivered. *Gilbert* [1877] may have been the first to recognize that as rivers are forced to carry increasing amounts of sediment, they lose energy capable of either lifting additional debris from the bottom of the river or eroding its bedrock channel. In unglaciated catchments, sediment carried in any river reach is transported to the particular reach from upstream tributaries and from adjacent hillslopes. In rivers with glacial headwaters, the quantity of sediment delivered to the top of the fluvial system can be huge, and will depend strongly on the footprint of the glacier. In clean-bedded alpine glacial settings, sediment produced from erosion of the glacier bed is swept from the glacier bed by efficient pressurized conduit systems. Ignoring long-term sediment storage at the bed, the discharge of sediment will be the integral of the erosion rate over the glacial footprint. Crudely, the sediment discharge is the product of a typical erosion rate with the glacial footprint. Sediment can aggrade so deeply that the river is prevented from eroding its bedrock channel floor during peak glaciation. This effect, documented in the Marsyandi River of Nepal by *Pratt et al.* [2002], is a possible deterrent of fluvial erosion in Kings Canyon in the last 1.5 Ma [*Stock et al.*, 2004], and was implicated in the origin of strath terraces in models of *Hancock and Anderson* [2002].

[47] We conclude by reemphasizing the dramatic differences between fluvial and glacial valleys. That the signature of glacial occupation of now deglaciated valleys remains so strong after 10–20 ka since the last glacial maximum implies that fluvial incision in the headwaters is inefficient relative to glacial incision. As first discussed a century ago by *Penck* [1905], the fundamental reason for the distinctive glacial signature is the pattern in ice discharge, which, in contrast to the fluvial system, increases to a maximum and then declines to zero. The pattern pivots about the ELA, which in turn has varied widely over the ice ages. The strongest control on the pattern of erosion is the distribution of ELAs, which range between LGM and present conditions, and where it intersects the topography. Expanding on *Porter*'s [1989] point, it is not only the mean Quaternary condition that dictates the shape of the glacial landscape, but the full distribution of Quaternary climates.

Appendix A

[48] While our approach in the main text has been to treat climate variability in a probabilistic manner, one can also
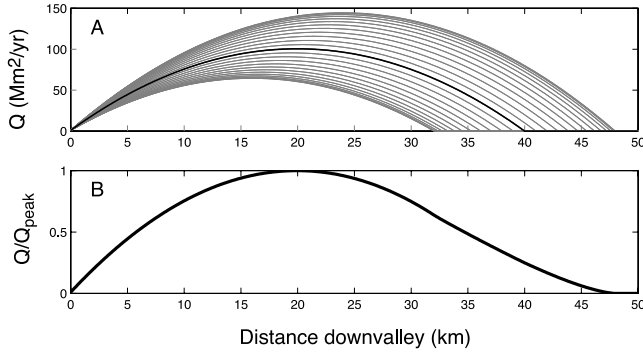
Figure A1. Numerical and analytic solutions for long-term average ice discharge when forced with harmonic history of ELA. (a) Solutions for ice discharge pattern for each of 20 times within the history of ELA. Thick line depicts ice discharge for mean ELA. (b) Numerical summation of discharge, normalized by peak discharge, corresponds exactly to analytical solution for long-term ice discharge using equation (A6).

cast the problem as a history over which we must sum the erosion. Here we present analytic results for the special case of a harmonically varying climate (Figure A1). Suppose that climate varies such that the ELA varies harmonically, $z_{ela} = z_0 - \Delta z \cos \omega t$, where z_0 is the mean ELA, Δz is the amplitude of its variation about the mean, and ω is the frequency of the oscillation. Then

$$b(x,t) = \gamma(z_{max} - z_0 + \Delta z \cos \omega t - Sx) \qquad (A1)$$

The equation for ice discharge becomes

$$Q(x,t) = W\gamma \left[(z_{max} - z_0 + \Delta z \cos \omega t)x - \frac{Sx^2}{2} \right],$$
$$\qquad (A2a)$$
$$x \leq x_L = \frac{2(z_{max} - z_0 + \Delta z \cos \omega t)}{S}$$

$$Q(x,t) = 0, \quad x \geq x_L \qquad (A2b)$$

[49] We seek the average erosion of a glacier whose flux and length vary with time so that along part of the valley the glacier is present during only part of the glacial cycle:

$$\overline{Q} = \frac{\omega}{2\pi} \int_{-\frac{\pi}{\omega}}^{\frac{\pi}{\omega}} Q(x,t)dt = \frac{\omega}{\pi} \int_{0}^{\frac{\pi}{\omega}} Q(x,t)dt \qquad (A3)$$

We recognize that during part of the cycle $Q = 0$, and the duration of that cycle depends upon the elevation of the point relative to the mean ELA and to the amplitude of the cycle. Where ice is always present, integrating (A5) yields, an expression similar to (7)

$$\overline{Q} = \frac{\omega}{\pi} \int_{0}^{\frac{\pi}{\omega}} Q(x,t)dt$$
$$= W\gamma \left[(z_{max} - z_0)x - \frac{Sx^2}{2} \right], \ x \leq 2(z_{max} - z_0 - \Delta z)/S \qquad (A4)$$

Where ice is present only part of the time at $x \geq 2(z_{max} - z_0 - \Delta z)/S$, however, the limits of integration are given by

$$0 \leq t \leq \frac{1}{\omega} \arccos \left[\frac{Sx - 2(z_{max} - z_0)}{2\Delta z} \right] \qquad (A5)$$

Using $\vartheta = \arccos \left[\frac{Sx - 2(z_{max} - z_0)}{2\Delta z} \right]$, (A5) becomes

$$\overline{Q} = \frac{\omega}{\pi} \int_{0}^{\frac{\vartheta}{\omega}} Q(x,t)dt$$
$$= W\gamma \left\{ \left[(z_{max} - z_0)x - \frac{Sx^2}{2} \right] \frac{\vartheta}{\pi} + \Delta z x \cos \omega t \sin \vartheta \right\} \qquad (A6)$$

Note that (A6) applies when glaciers are present only part of the time, and therefore when the ELA reaches or rises above the divide (z_{max}), including the case when its mean elevation is the higher ($z_0 > z_{max}$).

References

Anderson, R. S. (2000), A model of ablation-dominated medial moraines and the generation of debris-mantled glacier snouts, *J. Glaciol.*, 46(154), 459–469.

Anderson, R. S., C. A. Riihimaki, E. B. Safran, and K. R. MacGregor (2006), Facing reality: Late Cenozoic evolution of smooth peaks, glacially ornamented valleys and deep river gorges of Colorado's Front Range, in *Tectonics, Climate and Landscape Evolution*, edited by S. D. Willett et al., *Spec. Pap. Geol. Soc. Am.*, 398, 397–418.

Elvehoy, H., N. Haakensen, M. Kennett, B. Kjollmoen, J. Kohler, and A. M. Tvede (1997), Glasiologiske undersokelser i Norge 1994 og 1995, *Publ. 19*, Norges Vassdrags og Energiverk, Oslo.

Furbish, D. J., and J. T. Andrews (1984), The use of hypsometry to indicate long-term stability and response of valley glaciers to changes in mass transfer, *J. Glaciol.*, 30(105), 199–211.

Gilbert, G. K. (1877), *Report on the Geology of the Henry Mountains*, U.S. Gov. Print. Off., Washington, D. C.

Hallet, B., L. Hunter, and J. Bogen (1996), Rates of erosion and sediment evacuation by glaciers: A review of field data and their implications, *Global Planet. Change*, 12(1–4), 213–235.

Hancock, G. S., and R. S. Anderson (2002), Numerical modeling of fluvial terrace formation in response to oscillating climate, *Geol. Soc. Am. Bull.*, 114(9), 1131–1142.

Harbor, J. M. (1992), Numerical modeling of the development of U-shaped valleys by glacial erosion, *Geol. Soc. Am. Bull.*, 104, 1364–1375.

Harbor, J. M., B. Hallet, and C. F. Raymond (1988), A numerical model of landform development by glacial erosion, *Nature*, 333, 347–349.

Harrison, W. D., D. H. Elsberg, K. A. Echelmeyer, and R. M. Krimmel (2001), On the characterization of glacier response by a single time-scale, *J. Glaciol.*, 47, 659–664.

Johannesson, T., C. F. Raymond, and E. D. Waddington (1989), A simple method for determining the response time of glaciers, in *Glacier Fluctuations and Climatic Change*, edited by J. Oerlemans, pp. 343–352, Springer, New York.

MacGregor, K. R., R. S. Anderson, S. P. Anderson, and E. D. Waddington (2000), Numerical simulations of glacial-valley longitudinal profile evolution, *Geology*, 28, 1031–1034.

Meier, M. F., and A. Post (1962), Recent variations in mass net budgets of glaciers in western North America, *Int. Assoc. Hydrol. Sci. Publ.*, 58, 63–77.

Meier, M. F., W. T. Tangborn, L. R. Mayo, and A. Post (1992), Combined ice and water balances of Gulkana and Wolverine Glaciers, Alaska, and South Cascade Glacier, Washington, 1965 and 1966 Hydrologic years, *U.S. Geol. Serv. Prof. Pap.*, 715-A1971.

Oerlemans, J. (1984), Numerical experiments on large-scale glacial erosion, *Z. Gletscherkd. Glazialgeol.*, 20, 107–126.

Oerlemans, J., and J. P. F. Fortuin (1992), Sensitivity of glaciers and small ice caps to greenhouse warming, *Science*, *258*, 115–117.

Paterson, W. S. B. (1994), *The Physics of Glaciers*, 3rd ed., 480 pp., Elsevier, New York.

Penck, A. (1905), Glacial features in the surface of the Alps, *J. Geol.*, *13*, 1–19.

Porter, S. C. (1975), Equilibrium-line altitudes of late Quaternary glaciers in the Southern Alps, New Zealand, *Quat. Res.*, *5*, 27–47.

Porter, S. C. (1977), Present and past glaciation thresholds in the Cascade Range, Washington, USA: Topographic and climatic controls, and paleo-climatic implications, *J. Glaciol.*, *18*, 101–116.

Porter, S. C. (1989), Some geological implications of average Quaternary glacial conditions, *Quat. Res.*, *32*, 245–261.

Pratt, B., D. W. Burbank, A. Heimsath, and T. Ojha (2002), Impulsive alluviation during early Holocene strengthened monsoons, central Nepal Himalaya, *Geology*, *30*, 911–914.

Raymo, M. E. (1994), The initiation of Northern Hemisphere glaciation, *Annu. Rev. Earth Planet. Sci.*, *22*, 353–383.

Stock, G. M., R. S. Anderson, and R. C. Finkel (2004), Cave sediments reveal pace of landscape evolution in the Sierra Nevada, California, *Geology*, *32*(3), 193–196, doi:10.1130/G20197.1.

Sugden, D. E., and B. S. John (1976), *Glaciers and Landscape*, Edward Arnold, London.

Zachos, J., M. Pagani, L. Sloan, E. Thomas, and K. Billups (2001), Trends, rhythms, and aberrations in global climate 65 Ma to present, *Science*, *292*, 686–693.

_____

R. S. Anderson and M. A. Kessler, Institute for Arctic and Alpine Research, University of Colorado, 1560 30th Street, Campus Box 450, Boulder, CO 80309, USA. (robert.s.anderson@colorado.edu)

P. Molnar, Cooperative Institute for Research in Environmental Sciences, University of Colorado, Boulder, CO 80309, USA.